JOURNAL OF Applied Polymer SCIENCE

Special Issue: Bio-based Packaging

Guest Editors: José M. Lagarón, Amparo López-Rubio, and María José Fabra
Institute of Agrochemistry and Food Technology of the Spanish Council for Scientific Research

EDITORIAL

REVIEWS

RESEARCH ARTICLES

JOURNAL OF Applied Polymer SCIENCE

Special Issue: Bio-based Packaging

Guest Editors: José M. Lagarón, Amparo López-Rubio, and María José Fabra
Institute of Agrochemistry and Food Technology of the Spanish Council for Scientific Research

Impact of fermentation residues on the thermal, structural, and rheological properties of polyhydroxy(butyrate-*co*-valerate) produced from cheese whey and olive oil mill wastewater
L. Hilliou, D. Machado, C. S. S. Oliveira, A. R. Gouveia, M. A. M. Reis, S. Campanari, M. Villano and M. Majone, *J. Appl. Polym. Sci.* 2015, DOI: 10.1002/app.42818

Synergistic effect of lactic acid oligomers and laminar graphene sheets on the barrier properties of polylactide nanocomposites obtained by the in situ polymerization pre-incorporation method
J. Ambrosio-Martín, A. López-Rubio, M. J. Fabra, M. A. López-Manchado, A. Sorrentino, G. Gorrasi and J. M. Lagarón, *J. Appl. Polym. Sci.* 2015, DOI: 10.1002/app.42661

Antibacterial poly(lactic acid) (PLA) films grafted with electrospun PLA/allyl isothiocyanate fibers for food packaging
H. H. Kara, F. Xiao, M. Sarker, T. Z. Jin, A. M. M. Sousa, C.-K. Liu, P. M. Tomasula and L. Liu, *J. Appl. Polym. Sci.* 2015, DOI: 10.1002/app.42475

Poly(L-lactide)/ZnO nanocomposites as efficient UV-shielding coatings for packaging applications
E. Lizundia, L. Ruiz-Rubio, J. L. Vilas and L. M. León, *J. Appl. Polym. Sci.* 2015, DOI: 10.1002/app.42426

Effect of electron beam irradiation on the properties of polylactic acid/montmorillonite nanocomposites for food packaging applications
M. Salvatore, A. Marra, D. Duraccio, S. Shayanfar, S. D. Pillai, S. Cimmino and C. Silvestre, *J. Appl. Polym. Sci.* 2015, DOI: 10.1002/app.42219

Preparation and characterization of linear and star-shaped poly L-lactide blends
M. B. Khajeheian and A. Rosling, *J. Appl. Polym. Sci.* 2015, DOI: 10.1002/app.42231

Mechanical properties of biodegradable polylactide/poly(ether-block-amide)/thermoplastic starch blends: Effect of the crosslinking of starch
L. Zhou, G. Zhao and W. Jiang, *J. Appl. Polym. Sci.* 2015, DOI: 10.1002/app.42297

Interaction and quantification of thymol in active PLA-based materials containing natural fibers
I. S. M. A. Tawakkal, M. J. Cran and S. W. Bigger, *J. Appl. Polym. Sci.* 2015, DOI: 10.1002/app.42160

Graphene-modified poly(lactic acid) for packaging: Material formulation, processing, and performance
M. Barletta, M. Puopolo, V. Tagliaferri and S. Vesco, *J. Appl. Polym. Sci.* 2015, DOI: 10.1002/app.42252

Edible films based on chia flour: Development and characterization
M. Dick, C. H. Pagno, T. M. H. Costa, A. Gomaa, M. Subirade, A. De O. Rios and S. H. Flóres, *J. Appl. Polym. Sci.* 2015, DOI: 10.1002/app.42455

Influence of citric acid on the properties and stability of starch-polycaprolactone based films
R. Ortega-Toro, S. Collazo-Bigliardi, P. Talens and A. Chiralt, *J. Appl. Polym. Sci.* 2015, DOI: 10.1002/app.42220

Bionanocomposites based on polysaccharides and fibrous clays for packaging applications
A. C. S. Alcântara, M. Darder, P. Aranda, A. Ayral and E. Ruiz-Hitzky, *J. Appl. Polym. Sci.* 2015, DOI: 10.1002/app.42362

Hybrid carrageenan-based formulations for edible film preparation: Benchmarking with kappa carrageenan
F. D. S. Larotonda, M. D. Torres, M. P. Gonçalves, A. M. Sereno and L. Hilliou, *J. Appl. Polym. Sci.* 2015, DOI: 10.1002/app.42263

JOURNAL OF Applied Polymer SCIENCE

Special Issue: Bio-based Packaging

Guest Editors: José M. Lagarón, Amparo López-Rubio, and María José Fabra
Institute of Agrochemistry and Food Technology of the Spanish Council for Scientific Research

Structural and mechanical properties of clay nanocomposite foams based on cellulose for the food packaging industry
S. Ahmadzadeh, J. Keramat, A. Nasirpour, N. Hamdami, T. Behzad, L. Aranda, M. Vilasi and S. Desobry, *J. Appl. Polym. Sci.* 2015, DOI: 10.1002/app.42079

Mechanically strong nanocomposite films based on highly filled carboxymethyl cellulose with graphene oxide
M. El Achaby, N. El Miri, A. Snik, M. Zahouily, K. Abdelouahdi, A. Fihri, A. Barakat and A. Solhy, *J. Appl. Polym. Sci.* 2015, DOI: 10.1002/app.42356

Production and characterization of microfibrillated cellulose-reinforced thermoplastic starch composites
L. Lendvai, J. Karger-Kocsis, Á. Kmetty and S. X. Drakopoulos, *J. Appl. Polym. Sci.* 2015, DOI: 10.1002/app.42397

Development of bioplastics based on agricultural side-stream products: Film extrusion of *Crambe abyssinica*/wheat gluten blends for packaging purposes
H. Rasel, T. Johansson, M. Gällstedt, W. Newson, E. Johansson and M. Hedenqvist, *J. Appl. Polym. Sci.* 2015, DOI: 10.1002/app.42442

Influence of plasticizers on the mechanical and barrier properties of cast biopolymer films
V. Jost and C. Stramm, *J. Appl. Polym. Sci.* 2015, DOI: 10.1002/app.42513

The effect of oxidized ferulic acid on physicochemical properties of bitter vetch (*Vicia ervilia*) protein-based films
A. Arabestani, M. Kadivar, M. Shahedi, S. A. H. Goli and R. Porta, *J. Appl. Polym. Sci.* 2015, DOI: 10.1002/app.42894

Effect of hydrochloric acid on the properties of biodegradable packaging materials of carboxymethylcellulose/poly(vinyl alcohol) blends
M. D. H. Rashid, M. D. S. Rahaman, S. E. Kabir and M. A. Khan, *J. Appl. Polym. Sci.* 2015, DOI: 10.1002/app.42870

Journal of Applied Polymer Science

Structural and mechanical properties of clay nanocomposite foams based on cellulose for the food-packaging industry

Safoura Ahmadzadeh,[1] Javad Keramat,[1] Ali Nasirpour,[1] Nasser Hamdami,[1] Tayebeh Behzad,[2] Lionel Aranda,[3] Michel Vilasi,[3] Stephane Desobry[4]

[1]Department of Food Science and Technology, College of Agriculture, Isfahan University of Technology, Isfahan 84156-83111, Iran

[2]College of Chemical Engineering, Isfahan University of Technology, Isfahan 84156-83111, Iran

[3]Faculté des Sciences et Technologies, Institut Jean Lamour, Université de Lorraine, Boîte Postal (BP) 70239, F-54506 Vandœuvre-lès-Nancy, France

[4]Laboratoire d'Ingénierie des Biomolécules, École Nationale Supérieure d' Agronomie et des Industries Alimentaires, Université de Lorraine, 2 Avenue de la Forêt de Haye, Tri spécial à l'arrivée (TSA) 40602, 54518 Vandœuvre-lès-Nancy Cedex, France

Correspondence to: S. Ahmadzadeh (E-mail: s.ahmadzadeh@ag.iut.ac.ir)

ABSTRACT: In this work, an extensive study was carried out on the preparation and characterization of nanoclay biocomposites based on cellulose to substitute for synthetic polymer foam trays as food-packaging materials. The preparation stage was performed via a dissolution/regeneration route followed by drying with lyophilization. The chemical, physical, mechanical, and morphological properties of the prepared composite foams were characterized by several methods, including scanning electron microscopy, X-ray diffraction, Fourier transform infrared spectroscopy, mechanical tests, density, and color analyses. The obtained results indicate that the presence of nanoclay in the cellulose matrix caused more uniformity in the structure of the foams. Also, an increase in the nanoclay content resulted in a higher density, compressive strength, and Young's modulus. The achievements from this study suggest that the prepared cellulose nanocomposite foam could be a potential alternative to commercial synthetic foams for packing food products.
 J. Appl. Polym. Sci. **2016**, *133*, 42079.

KEYWORDS: cellulose and other wood products; clay; composites; foams; packaging

Received 25 November 2014; accepted 6 February 2015
DOI: 10.1002/app.42079

INTRODUCTION

Cellular structures with internal textures of microporosity to macroporosity are made on the basis of mineral or organic materials.[1] These kinds of porous structures are used for different applications, such as packaging and insulating. Plastics and foams are the most important materials used to produce disposable packaging for foodstuffs because they are lightweight and heat insolent.[2] The main characteristics of packaging materials, including their mechanical and barrier properties, depend on their structures. In current methods of foam production, a blowing agent is mixed under pressure with different mixtures, such as a liquid polymer or monomer mixture, and ultimately, foams are prepared by pressure release, a proper temperature increase, or chemical reaction. Subsequently, the foam is rigidified by the reduction of the temperature or the crosslinking of the monomers. Macroporous foams will be achieved by these methods because of uncontrolled nucleation, which causes growth and aging of the bubbles.[2] The sol–gel method is a widely investigated approach in the preparation of porous materials.[3] In this method, aerogel-like materials are formed by the replacement of liquid in a gel with a high volume gas percentage (80–99.8% of the total volume) and are finally recognized as nanoporous solids with a limited shrinkage. Aerogels have a porous low-density structure and are quite ductile and mechanically robust.[4]

In some cases, parts of food-packaging materials, such as glass and paper, can be easily recovered; however, in other industries, such as the meat, poultry, or seafood industry, the recycling of packaging materials is difficult because the materials need some washing, which may not be available before recycling and which will add more expenses. Thus, the use of biodegradable materials seems to be more feasible.

Nowadays, cellular materials from biopolymers have attracted much attention for different applications, especially where biodegradability and biocompatibility are in demand, such as in green packaging, insulating materials, delivery matrices, and tissue engineering.[5] However, despite all of the advantages of using

Table I. Some of the Earlier Studies Related to Cellulose Nanocomposite Aerogels and Films

	Subject	Solvent/method	Reference
Aerogels	Cellulose microfiber–nanofiber–zeolite nanocomposites	Freeze drying	Bendahou *et al.*[11]
	Cellulose–SiO_2 nanocomposites	NaOH/thiourea solution, freeze drying	Shi *et al.*[12]
	All-cellulose nanocomposites	8 wt % LiCl/Dimethylacetamide (DMAc) solution, freeze drying	Duchemin *et al.*[13]
	Cellulose whisker/MMT nanocomposites	Dispersion of cellulose whiskers into the water, freeze drying	Gawryla *et al.*[14]
Films	Cellulose/$CaCO_3$ bionanocomposites	NaOH/urea solution	Jia *et al.*[15]
	Cellulose–clay layered nanocomposite	LiOH/urea solution	Yang *et al.*[16]
	Nanocrystalline cellulose/cellulose nanocomposite	Functionalized ionic liquid solution	Ma *et al.*[17]

biopolymers, there are some shortcomings in their performance that should be improved. One of the proposed alternatives is the incorporation of nanoparticles into the matrix of biopolymers; these nanoparticles reinforce the mechanical, thermal, and barrier properties of the biopolymers. Montmorillonite (MMT) is the most widely used type of nanoparticle in polymer nanocomposites. It is a reinforcing material and is naturally abundant, nontoxic, inexpensive, and chemically and thermally stable. Also, because of its platelike shape, it can be a proper choice for reducing the cell size and improving the foam structure. Therefore, it can be used as a component in food-packaging, medical, and other applications.

In the last decade, the preparation of porous materials based on some kinds of polysaccharides, such as agar, hydroxypropyl cellulose, silk fibroin, and cellulose, has been investigated. Cellulose, as one of the most important natural biopolymers, can be the best option, with a special potential to prepare multifunctional materials.[5] Regenerated cellulose products have shown some attractive properties, including a fascinating structure, biocompatibility, biodegradability, and derivable properties that introduce them as potential biodegradable packaging materials.[6,7] The preparation of porous cellulose with different solvents and methods has been previously reported.[1,4,5,8,9] Sescousse *et al.*[9] prepared aerocellulose from cellulose ionic liquid solutions and compared the properties with those obtained from cellulose–NaOH and cellulose–NMMO routes. After the cellulose gels were made, they were dried under supercritical CO_2 conditions to prepare aerocellulose. Fischer *et al.*[1] synthesized cellulose-based aerogels by crosslinking cellulose acetate with a nontoxic isocyanate via the sol–gel method using a tin-based catalyst. Moreover, the preparation of composite foams from vegetable raw materials, such as starch, cellulose, fibers, and vegetable proteins that are of relatively low cost and are renewable resources widely found in nature, has been reported.[10] Depending on the required properties of the porous materials, different reinforcing approaches, such as the preparation of composite materials, the insertion of a second polymer, or the incorporation of organic and inorganic materials, and crosslinking are used. However, the use of these techniques for cellulose aerogels needs more research, and also, the improvement of the mechanical properties of cellulose aerogels along with the preservation of the high porosity of these materials is a challenging task. Some of the studies on cellulose nanocomposite aerogels and also some of the studies on the preparation of cellulose nanocomposite films are presented in Table I.

There are many potential applications for cellulose aerogels, and they require specific cell structures. Several techniques, such as the addition of a surfactant and the use of salts, carbon nanotubes, paraffin, and so on, have been developed to control the cell size and morphology of aerogels.[18–20] Therefore, the major goal of this study was done to investigate the effects of both the surfactant and nanoclay on the cell structure, to reduce the pore sizes to prepare nanofoams, and to enhance the mechanical, thermal, and barrier properties of the aerogels for use in packaging applications. Because it has been illustrated that the formation of a uniform structure with smaller cell sizes is one of the most important factors in foam production which affecting strongly mechanical properties.

In this study, the influence of surface-modified montmorillonite (SM-MMT) as nanofiller, and the effect of surfactant on foam properties were investigated. The density, porosity, morphology, and mechanical properties of prepared foams were characterized. The obtained results showed that the presence of SM-MMT caused more uniformity in the structure of cellulose foams. Moreover, the mechanical properties were enhanced by incorporation of nanoparticles into the cellulose matrix.

EXPERIMENTAL

Materials

In this study, Avicel PH-101 microcrystalline cellulose (MCC) with the crystallinity index of about 66%, and SM-MMT containing 25–30 wt % methyl dihydroxyethyl hydrogenated tallow ammonium were purchased from Sigma–Aldrich. Also, Tween 80 surfactant (>98% purity) was obtained from Sigma-Aldrich. All other chemicals (analytical grade) were purchased from local commercial sources and did not undergo any pretreatment.

Sample Preparation

The cellulose solution preparation procedure was reported previously.[21] Cellulose solutions were prepared in several stages

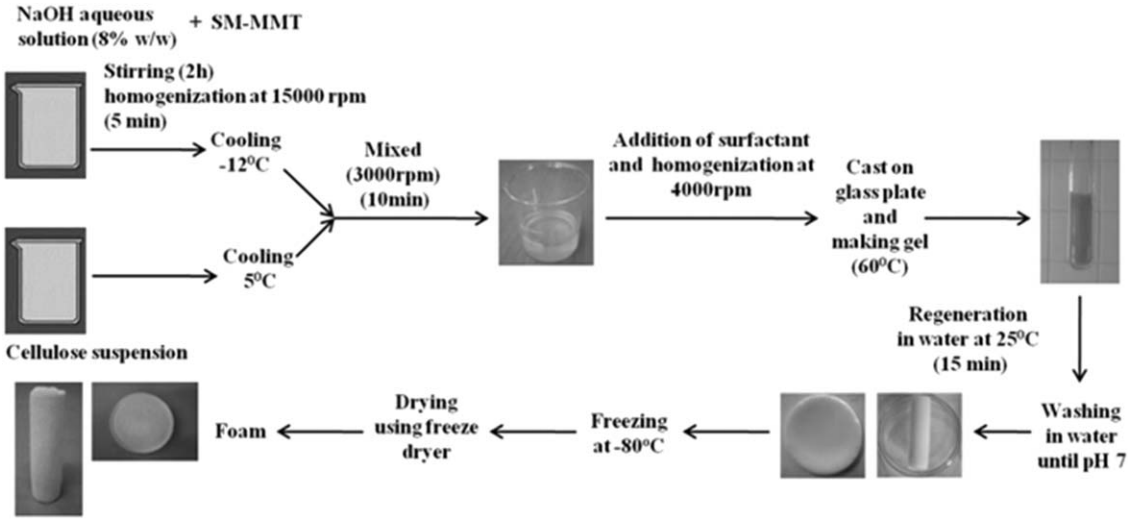

Figure 1. Schematic for the preparation of the nanocomposite cellulose foam.

(Figure 1). Briefly, a 8 wt % NaOH aqueous solution was prepared. A desired amount of SM-MMT was added to this solution and was then dispersed with 2 h of stirring at room temperature. The prepared suspension was further homogenized at 15,000 rpm for 5 min with an Ultra-Turrax T25 homogenizer (IKA, Germany),[22] and it was then cooled down to −12°C. Simultaneously, the swollen cellulose was prepared in distilled water and cooled to 5°C. Afterward, the dissolution of cellulose was performed by the addition of swollen cellulose to an SM-MMT suspension at −12°C and then vigorous mixing at 3000 rpm for 10 min. Then, various concentrations of Tween 80 (0.1, 0.6, and 1.1%) were added to the suspension. Stirring was then performed at 4000 rpm for 5 min at ambient temperature. The solutions were then poured into Petri dishes in 2 mm thick layers and also into cylindrical molds to a height of 5 cm. The gelation process of the cellulose solution was performed at 60°C for 1 h. In the next step, the gel was immersed in a water coagulation bath at 25°C, and then, the solidified gel was washed in a water-regenerating bath to remove all solvent. The quality of the precipitation in this process depended on the solvent power, cellulose concentration, and interaction strength between the solvent and nonsolvent.[8,23] Finally, after the gels were frozen at −80°C, a freeze dryer (Lyophilisateur ALPHA 1–2/LD) was used to dry the samples.[9,16,24] After lyophilization, dry samples whose colors were slightly different on the basis of the amount of SM-MMT were obtained.[4] The weight ratios of cellulose and SM-MMT in the composite foams under investigation were 100:0, 97.5:2.5, 95:5, and 90:10; these foams were denoted as CN0, CN2.5, CN5, and CN10, respectively. The conditioning of the foams was performed at 20°C and 50% relative humidity for 48 h before characterization.

Characterization of SM-MMT and MCC

To analyze and observe the morphology of the SM-MMT particles and cellulose crystals, several methods, including scanning electron microscopy (SEM), X-ray diffraction (XRD; X'Pert Philips diffractometer), and Fourier transform infrared (FTIR) analyses, were used.

Foam Characterization

SEM. SEM images were taken with a Hitachi S4160 cold field emission scanning electron microscope at an acceleration voltage of 20 kV. To prevent electrical charging during SEM investigations, thin layers of gold were deposited by sputtering onto the surface and the cross section of the samples.

Density and Porosity Measurements. The bulk density (ρ_b) was determined by the division of the weight by volume of the samples. To calculate the volume of the foams, the dimensions were measured with a vernier caliper.[9,25] The solid density (ρ_s) was determined with an Accupyc 1330 helium pycnometry apparatus. The apparent porosity (ε) and global specific porous volumes (V_p) were calculated according to the following equations:[1]

$$\varepsilon = 1 - \frac{\rho_b}{\rho_s}$$

$$V_p = \frac{1}{\rho_b} - \frac{1}{\rho_s}$$

Color Measurement. The foam color was analyzed with a spectrophotometer (Datacolor Industrial model 200, Lawrenceville, KS). A Lab color scale was used to measure the degree of lightness (L), redness ($+a$) or greenness ($-a$), and yellowness ($+b$) or blueness ($-b$) of the foams. The instrument was calibrated with two calibration plates. Pure cellulose foam was used as a reference with color coordinates of $L = 90.35$, $a = -0.06$, and $b = -0.65$. The total color difference for each sample (ΔE) was calculated according to the following equation:

$$\Delta E = [(L_{\text{foam}} - L_{\text{reference}})^2 + (a_{\text{foam}} - a_{\text{reference}})^2 + (b_{\text{foam}} - b_{\text{reference}})^2]^{0.5}$$

The mean of three measurements for each sample was reported as the final value.[26]

FTIR Spectroscopy. FTIR spectra were recorded with an FTIR Nicolet 8700 spectrometer (attenuated total reflection with a diamond crystal) equipped with an mercury cadmium telluride

(MCT) detector cooled by liquid nitrogen in the wavelength range from 4000 to 500 cm^{-1}.

XRD Studies. XRD measurement was carried out to evaluate the structure of the composite foams. The XRD patterns of the foams were obtained in the reflection mode. The recording of the spectra was performed in the range $2\theta = 3–75^\circ$ on a $\theta–2\theta$ type CGR θ 60 diffractometer (X'Pert Pro, Philips) with Kα radiation of a copper anticathode ($\lambda K\alpha 1 = 1.54056$ Å) at 40 kV and 40 mA, where θ is the diffraction angle in degrees.[24] Data collection was performed with a detector at a rate of $2\theta = 0.5^\circ$/min. The d-spacing of the SM-MMT layers was calculated with Bragg's equation ($d = n\lambda/2 \sin\theta$). The total degree of crystallinity (Cr) was estimated according to Rabek's method[27] with the following formula:

$$Cr = \frac{S_c}{S_c + S_a} \times 100\%$$

where S_c and S_a are the areas of the cellulose crystals and the amorphous regions, respectively. A peak-fitting process with a Gaussian function was performed to extract individual crystal peaks and the amorphous background.[16,17,28]

Compression Test. The dry samples were cylindrically cut, with the height being 1.5 times larger than the diameter for uniaxial compression test with a Lloyd universal testing machine (Lloyds EZ50, Lloyds Instruments, Ltd., United Kingdom) equipped with a 500-N load cell. The cylinder-shaped sample was inserted between two steel circular compression plates. A deformation rate of 20 mm/min was applied on the top surface of each specimen. All of the measurements were carried out under ambient conditions at about 20–22°C and 50–60% relative humidity. Young's modulus (E) was determined from the initial slope of the stress–strain plot. The absorption energy was defined as the area below the stress–strain curve from 0 to 40% strain.[4]

Statistical Analysis. An analysis of variance followed by an least significant difference (LSD) comparisons of means test ($p \leq 0.05$) was performed with PASW Statistics 18 software.

RESULTS AND DISCUSSION

Structural Characteristics of the Foams

The free surface of samples that was in contact with the coagulant and their cross section were observed with SEM (Figures 2 and 3). As shown Figure 2, the surfaces of all foams with different SM-MMT contents were completely compact because of skin formation as a result of high solvent elimination rate occurring during gel development [Figure 2(a)].

The fracture cross section of foams images were used to analyze the morphology of pores [Figure 3(a–h)]. As shown in images, the internal section of the foam had a heterogeneous porous structure. The observed difference in the structures was due to the effect of the SM-MMT contents and their distribution through the cellulose matrix. The pore walls thickness was estimated to be between 40–300 nm.

According to the results obtained from SEM images with ImageJ software analyzer, a wide pore diameter distribution range, between a few hundred nanometers and 2 μm, was observed in the pure cellulose foam (Figure 4). However, it was clear that the addition of a small amount of SM-MMT to the cellulose network could reduce the cell size significantly compared to that of the pure cellulose foams. The addition of SM-MMT also created a smaller range of pore size distributions (<100 to 700 nm; Figure 4).

This particular structure of cellulose foam with a wide range of pore sizes could be explained as follows. Opacity was created in the cellulose solutions during the gelation step; this indicated phase separation (the separation of the solvent from cellulose). Therefore, during the regeneration process, the dilution of free-solvent regions by water led to large pores. The rest of the solvent was then removed from cellulose, and small pores were created. In cases where the miscibility of solvent and cellulose was completely homogeneous all over the volume, the regeneration process separated cellulose from the solvent in one step.[5]

Cellulose/SM-MMT nanocomposite foams indicated a different porous structure compared to the cellulose/silica based aerogels that were prepared by Shi *et al.*[12] Gawryla *et al.*[14] reported that increasing the concentration of clay and cellulose caused a transition from layered architectures to three-dimensional porous structures. However, the large pores in both structures were observed.

To increase the porosity in the final structure of the foams, the surfactant Tween 80 was added to the solution at concentrations of 0.1, 0.6, and 1.1%. The effect of the surfactant concentration on the morphological properties of foams is represented in SEM images. As shown in the SEM images, the addition of surfactant to the CN0 solution created more large pores; this subsequently increased V_p (Table II) and decreased the density. The presence of surfactant improved the SM-MMT dispersion, and this led to the formation of more uniform structures with average pore sizes in the range of nanometers. The steric repulsion mechanism, because of the effect of Tween 80 as a nonionic surfactant, is one of the most important mechanisms that stabilize the aqueous dispersion of nanoparticles. The adsorption of nonionic surfactants on the surface of the nanoparticles occurs in compact mode; so, its efficiency to stabilize dispersion of nanoparticles is greater than that of the polymers.

Density and Porosity

The density and porosity of the nanocomposite foams as a function of the SM-MMT and surfactant concentrations are shown in Figure 5(a,b), respectively. These results are related to foams with different concentrations of SM-MMT or surfactant prepared under the same conditions. As expected, with an increase in the concentration of SM-MMT, the density increased. However, there was no linear dependence between the nanoclay concentration and the density. Our findings resembled the results reported by Gawryla *et al.*[14] and Shi *et al.*[12] for nanocomposite aerogels. Gawryla *et al.*[14] reported higher densities for cellulose whisker/clay aerogels compared to the pure samples, and Shi *et al.*[12] reported that the incorporation of SiO_2 reduced the porosity of cellulose composite aerogels. When the SM-MMT concentration was increased to 5%, the mean pore size diameter and, accordingly, V_p were decreased. Also, the pore size distribution was shifted to lower values (on the basis of the SEM images). Moreover, the incorporation of surfactant into the composite solutions

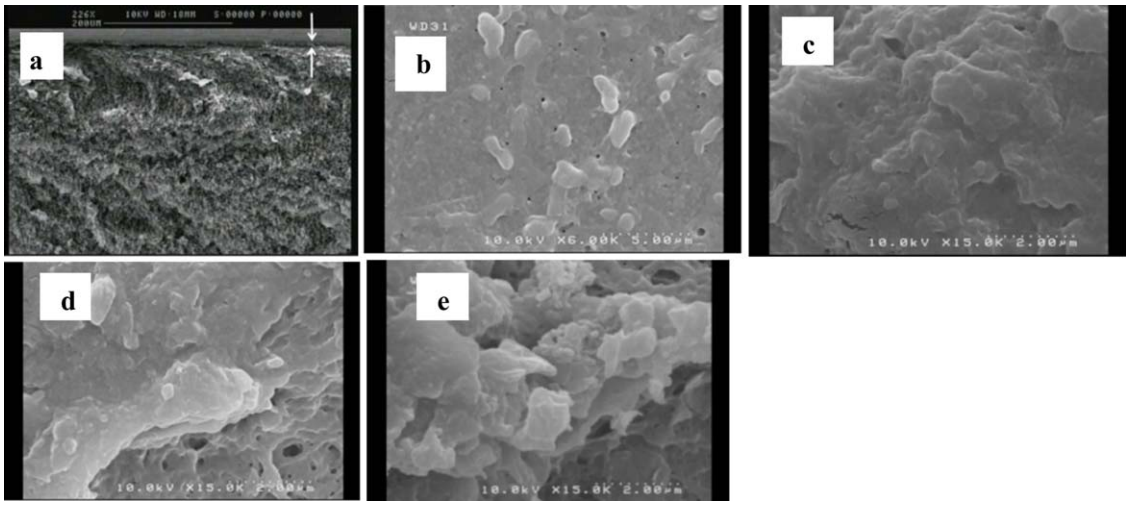

Figure 2. (a) Dense skin at the surface of the foam and (b–e) SEM images of the free surfaces of cellulose foams prepared from cellulose solutions (5 wt %) with different contents of SM-MMT (CN0, CN2.5, CN5, and CN10, respectively).

improved the dispersion of the SM-MMT nanoparticles; this subsequently reduced the cell sizes and V_p and led to an increase in the density.

Color

The color of foams ranged between white and cream, depending on the amount of SM-MMT. Table III shows the color parameters of the cellulose foams. Because the cellulose powder was white, the color of the pure cellulose foams was approximately white. Its slightly yellowish aspect could have been due to the effect of high temperatures during gelation, which caused some degradation.[26] An increase in the SM-MMT content had a significant effect on the color of the foams (Table III).

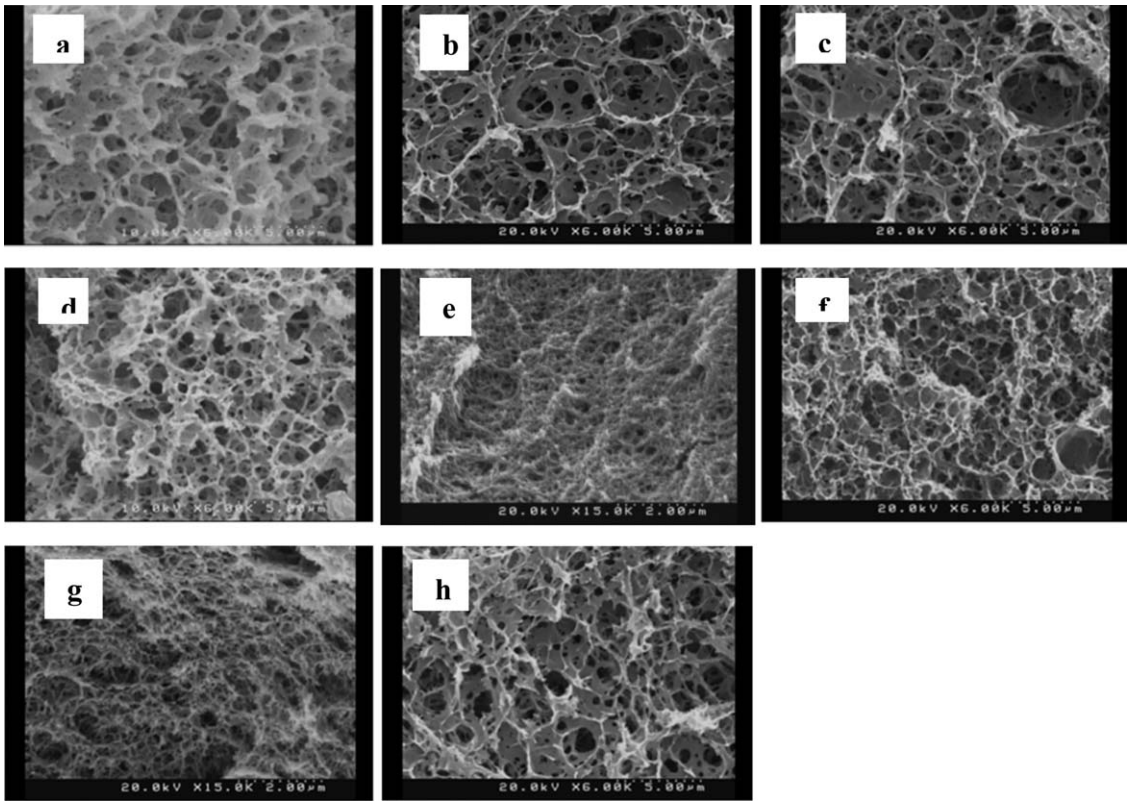

Figure 3. SEM images of the cross sections of cellulose foams prepared from cellulose solutions (5 wt %) with different contents of SM-MMT and Tween 80: CN0 with (a) 0.1, (b) 0.6, or (c) 1.1% Tween 80; CN2.5 with (d) 0.1 or (e) 0.6% Tween 80; CN5 with (f) 0.1 or (g) 0.6% Tween 80; and (h) CN10 with 0.1% Tween 80.

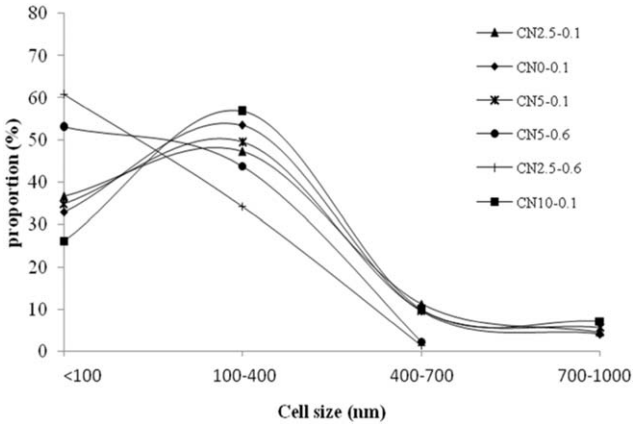

Figure 4. Average pore size distributions of the cellulose composite foams. The numbers in CN0, CN2.5, CN5, and CN10 indicate the surfactant concentration (%).

FTIR Spectroscopy

The FTIR spectra of the MCC, SM-MMT, and nanocomposite foams with different SM-MMT contents (CN0, CN2.5, CN5, and CN10) are shown in Figure 6(a–d). A peak at 1432 cm^{-1} was observed for the cellulose powder and was attributed to the cellulose I crystal, which disappeared in foams after dissolution in NaOH aqueous solution. This result indicates that the crystal structure of cellulose changed to cellulose II after regeneration.

For SM-MMT, four peaks at 1010 cm^{-1} (Si—O stretching), 1650 cm^{-1} (—OH bending, hydration), 1470 cm^{-1} (C—H bending modes of the functional groups present at the surface of the clay particles), and 3635 cm^{-1} (—OH stretching or Al—Al—OH stretching) and two peaks at 2850 and 2920 cm^{-1} (C—H stretching modes of the clay or the functional groups present at the surface of the clay) were observed. The main differences between the nanocomposite foams and cellulose were the appearance of new shoulders at 2923 and 2950 cm^{-1} from the C—H functional groups of the clay particles, new well-defined O—H stretching modes due to clay–cellulose interaction at 3490 and 3440 cm^{-1}, a new shoulder at 1470 cm^{-1} coming from the C—H functional groups of the clay particles, and also two new peaks at 895 and 924 cm^{-1}, which were due to the presence of clay (these peaks appeared at 883 and 917 cm^{-1} in the SM-MMT spectra) and shifted to higher wave numbers in the composites, with the assumption of stronger interactions between the cellulose matrix and SM-MMT. A small peak at 1620 cm^{-1}, corresponding to the bending vibrations of —OH groups, was observed for the nanocomposites.[29]

The wide peak at 3300 cm^{-1} indicated a change in the hydration structure of the foams compared to pure cellulose powder with more bonded H_2O molecules or O—H groups through hydrogen bonds, and the band at 3621 cm^{-1} revealed free O—H groups in the SM-MMT. This band disappeared in the spectra of the foams; this indicated that the free water in SM-MMT was replaced with new groups. According to the FTIR spectrum, cellulose chains and SM-MMT interacted through hydrogen bonds. So, we concluded that during the formation of the cellulose–SM-MMT nanocomposite foams, new hydrogen bonds were formed between the cellulose and SM-MMT nanoparticles. In general, the FTIR spectra confirmed the presence of SM-MMT in the cellulose matrix and the interactions between the SM-MMT and cellulose.[30]

XRD

To investigate the morphological structure of the SM-MMT particles (intercalated and exfoliated) in the nanocomposites, XRD analysis was used. The interlayer basal spacing of the clay mineral increased with the intercalation of the polymer chains and was recognizable by the diffraction peak with lower angle values. When an exfoliation nanocomposite structure was reached, a lack of order between the silicate layers caused the diffraction peaks to disappear from the XRD pattern. The XRD patterns of the MCC, SM-MMT, and nanocomposite foams (CN0, CN2.5, CN5, and CN10) are shown in Figure 7. These results indicated a shifting of the 2θ value to lower angle values in the nanocomposite foams; this could be explained by an increase in the *d*-spacing value via the cellulose and Tween 80 molecules entering between the silicate layers, although the intercalation of cellulose chains into the silicate layers was difficult because of their large molecular size. Moreover, we concluded from the decreasing 2θ values that the intercalated structure was created during the preparation of nanocomposite foams. Bragg's equation was used to convert the 2θ values to basal spacing values. An intense diffraction peak was observed in the SM-MMT pattern at a 2θ angle of 4.9; this corresponded to a clay interlayer spacing value of 1.8 nm. With the addition of nanoclay to the cellulose matrix to prepare nanocomposite foams, the detected peak for SM-MMT was shifted to a lower angle (Figure 7). The foams with 2.5 and 5% SM-MMT showed a peak at a 4.1° angle (*d*-spacing 2.1 nm) with less intensity. When the SM-MMT content was increased to 10%, the *d*-spacing decreased from 2.1

Table II. V_p and Crystallinity of the Nanocomposite Foams

	V_p (cm^3/g)			
	Tween 80%			
MMT (%)	0.1	0.6	1.1	Crystallinity (%)
0	10.15 ± 0.97^a	10.44 ± 1.22^a	12.94 ± 0.98^a	20.79
2.5	8.68 ± 0.05^b	7.24 ± 0.04^b	7.14 ± 0.04^b	26.91
5	5.94 ± 0.17^c	5.41 ± 0.18^c	5.25 ± 0.21^c	32.98
10	4.56 ± 0.14^d	4.53 ± 0.19^c	4.37 ± 0.40^c	34.59

In each column, the same superscript letters are not significantly different according to the LSD test ($p < 0.05$).

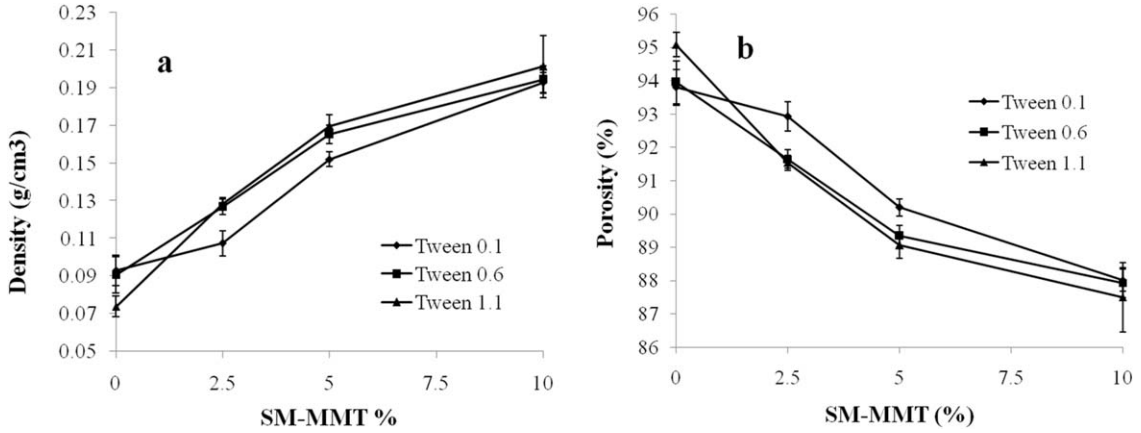

Figure 5. (a) Density and (b) porosity of cellulose nanocomposite foams as a function of the SM-MMT concentration.

to 1.9 nm. The XRD results also indicated that the Tween 80 surfactant significantly affected the dispersion of SM-MMT because of the adsorption on the surface of the particles and intercalation between the silicate layers of SM-MMT.[16,31]

The broadening and reduction of the peak intensity showed that the layered structure did not have one distinct space; this indicated that the clay was partially exfoliated. According to these results, a completely exfoliated morphology was not obtained because of the strong polar interactions between the hydroxyl groups in the cellulose chain. To reach a complete exfoliated nanocomposite structure, it was necessary that more chains of the polymer enter the clay galleries and push the layers further apart. In this case, a wider diffraction peak was observed in the patterns. This peak was broadened into the baseline when the exfoliation was completed.[30,32]

Chivrac *et al.*[33] and Chung *et al.*[34] observed similar behaviors for starch/SM-MMT thermoformed films, and in all cases, the nanocomposites presented an intercalated structure. Wilhelm *et al.*[35] and Majdzadeh-Ardakani *et al.*[36] obtained starch/SM-MMT nanocomposite films with an intercalated structure, as shown by their XRD patterns.

The type of cellulose crystals was determined with XRD patterns as well. During the regeneration stage, the native cellulose I crystal structure was dissolved in a solvent, and after precipitation in a nonsolvent, cellulose II was created as a different crystal structure.[4] Two obvious crystal peaks at $2\theta = 22.6$ and 14.98° of MCC, which were assigned to cellulose I crystals (Figure 8), were observed. However, the crystal peaks of the foams shifted to 12.24, 19.96, and 21.69° were assigned to the crystals of cellulose II.[37] The results obtained from XRD and FTIR spectroscopy revealed that the crystal structure of the cellulose foams transformed from cellulose I to cellulose II after dissolution in the NaOH aqueous solution and regeneration. The crystallinity values of the foam samples are shown in Table II. The crystallinity increased slightly compared to that of the original cellulose sample in the presence of SM-MMT.[6]

Compression Test

A uniaxial compression test of the nanocomposite foams was performed to compare the effect of SM-MMT on the mechanical properties. A typical stress–strain curve of the nanocomposite foams and their mechanical properties are shown in Figure 9. According to the stress–strain curve, the cellulose foams revealed strain-hardening behavior due to the bending of cellulose fibers compared to the polymer foams, which showed a flat region in the stress–strain curve (the increasing strain at the constant stress) and that behaved as an elastic–plastic material. There are two regions in this curve; the first part is the linear elastic region that could be used to calculate *E*. The second region has a lower slope that shows where the cell wall collapse occurred. The low slope of this region made the material able to absorb a significant amount of energy.[9] All characteristics obtained from the compression test were compared for different nanocomposite foams and analyzed as a function of the density. As demonstrated in Figure 9, the presence of SM-MMT led to a higher resistance to collapse; thus, a higher modulus is shown in the stress–strain curves. The lower ductility of the

Table III. Color Coordinates of the Nanocomposite Foams

MMT (%)	*L*	*a*	*b*	Δ*E*
0	90.61 ± 1.11	−0.07 ± 0.04	−0.44 ± 0.19	0
2.5	92.75 ± 1.07	−0.79 ± 0.11	3.56 ± 0.59	4.89 ± 0.46
5	91.58 ± 0.73	−0.85 ± 0.09	5.47 ± 0.53	6.11 ± 0.71
10	94.11 ± 0.89	−0.54 ± 0.08	6.35 ± 0.65	7.76 ± 0.56

The mean difference is significant at the 0.05 level.

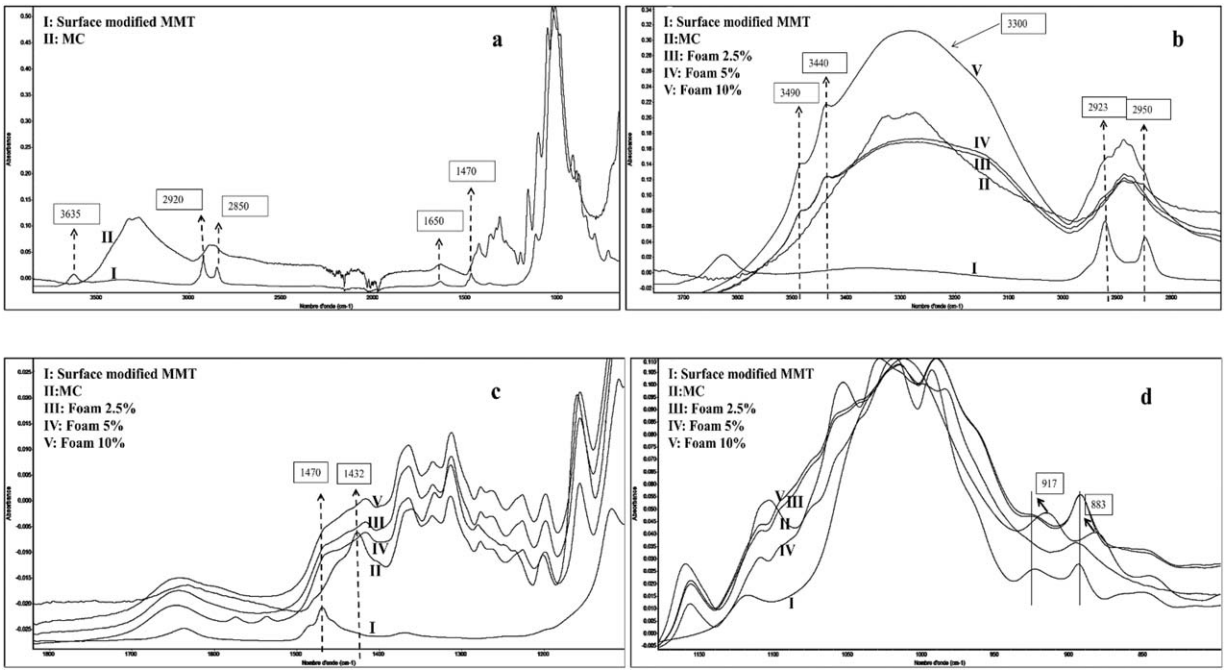

Figure 6. FTIR spectra of (a) Microcrystalline cellulose (MCC) and SM-MMT and (b–d) cellulose foam and pure cellulose nanocomposite foams.

nanocomposite foams was due to the presence of S-MMT particles in the cellulose matrix. These particles could not bend and subsequently increased the resistance of foams to bending and made them brittle. On the other hand, the modulus under pressure depended on the homogeneity of the structure. High uniformity in network causes the load to be carried efficiently, even at very low densities.[4,9] The SEM images indicated that the presence of SM-MMT in the cellulose matrix caused more uniformity in the structure of the foams.

The obtained results were in agreement with the findings of Bendahou *et al.*[11] and Gawryla *et al.*[14] They reported a higher stiffness, as measured by the compression *E* and compressive strength, for composite aerogels.

A relationship between the *E* values of the porous materials and their ρ_b values has been reported as follows:[9]

$$E \approx \rho^n$$

where *n* is the exponent in the relationship between *E* values and bulk density.

The value of *n* is dependent on the kind of material; for example, for open cell regular foam, the prediction of the model was $n \approx 2$ and for aerogels was expected to be higher ($n = 2.5$–4). This difference was due to the formation process. The relationship between *E* and density of foams is shown in Figure 10(a). In this study, the regeneration step was the main section of foam preparation, which could cause some defects in the structure, and accordingly, it was expected to show a behavior

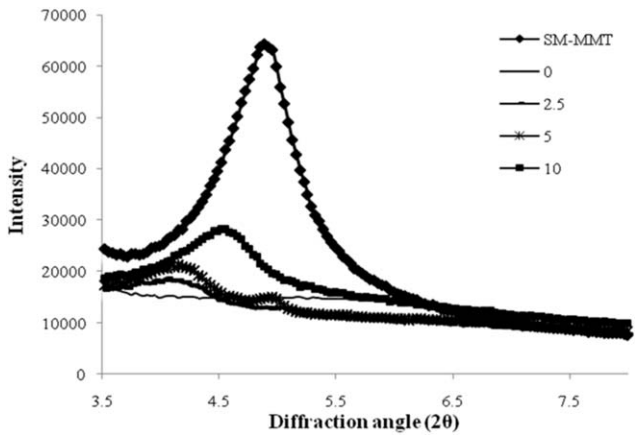

Figure 7. XRD patterns of SM-MMT, CN0, CN2.5, CN5, and CN10 ($2\theta = 4$–8).

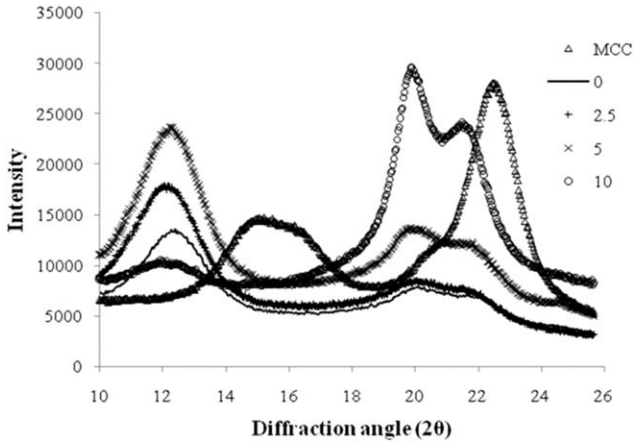

Figure 8. XRD patterns of MCC, CN0, CN2.5, CN5, and CN10 ($2\theta = 10$–26).

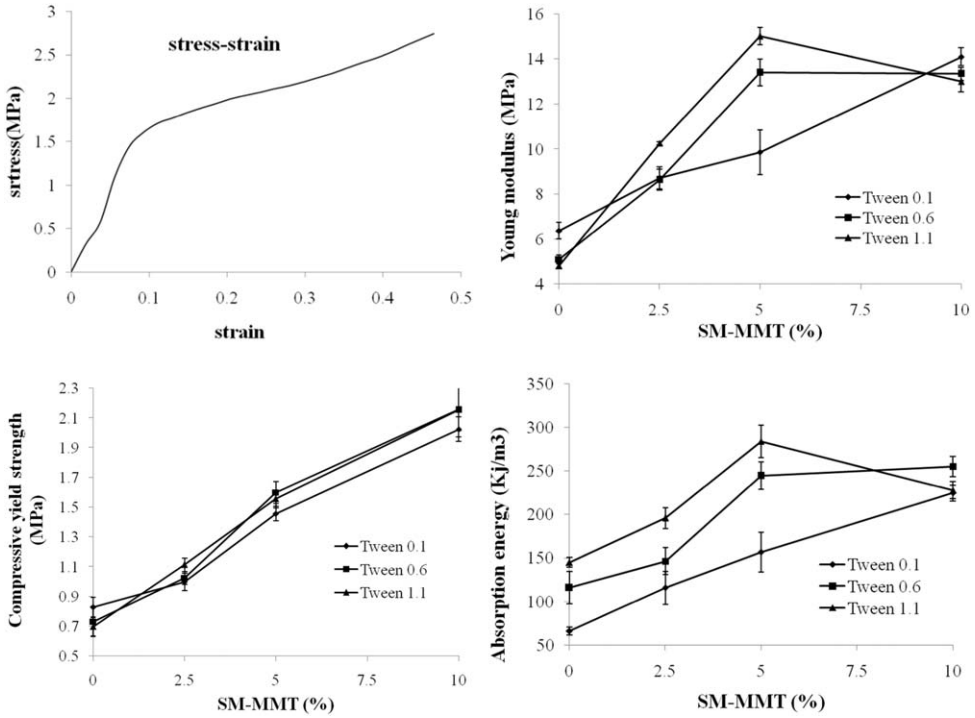

Figure 9. Typical stress–strain curve for the cellulose foam and *E*, compressive yield strength, and absorption energy values versus the SM-MMT concentration.

similar to the that of the aerogels. However, the scaling exponent was calculated to be 1.226, which was lower than the values reported for nanoporous cellulose materials in the literature, and its reason was not clear. As shown in the curve, the value of *n* was close to 1; this indicated that a linear model could explain the result in the range of 0.07–0.2 of the density. The correlation between the compressive yield strength with the foam density is presented in Figure 10. As expected, this parameter was increased with the addition of SM-MMT to the cellulose matrix.

The obtained results were comparable with the values reported by Sescousse *et al.*[9] for aerocellulose prepared with cellulose dissolution in an NaOH procedure. These results were slightly lower than the values reported for closed-cell synthetic polymer foams used for packaging.[10] Lawton *et al.*[38] prepared composite cornstarch foams by the addition of aspen fiber and reported an improvement in the mechanical properties with increasing fiber content of up to 15%. However, with the addition of a greater amount of fiber, the mechanical properties were weakened because of a lack of uniformity in distribution. Glenn *et al.*[39] and Soykeabkaew *et al.*[40] reported similar results for composite foams prepared from starch with the addition of softwood fiber and jute fibers, respectively.[10]

According to the mechanical properties, the fabricated materials obtained in this study could be used for applications, such as packaging or protection.

CONCLUSIONS

Biodegradable cellulose/SM-MMT nanocomposite foams were prepared via cellulose dissolution in NaOH/water followed by

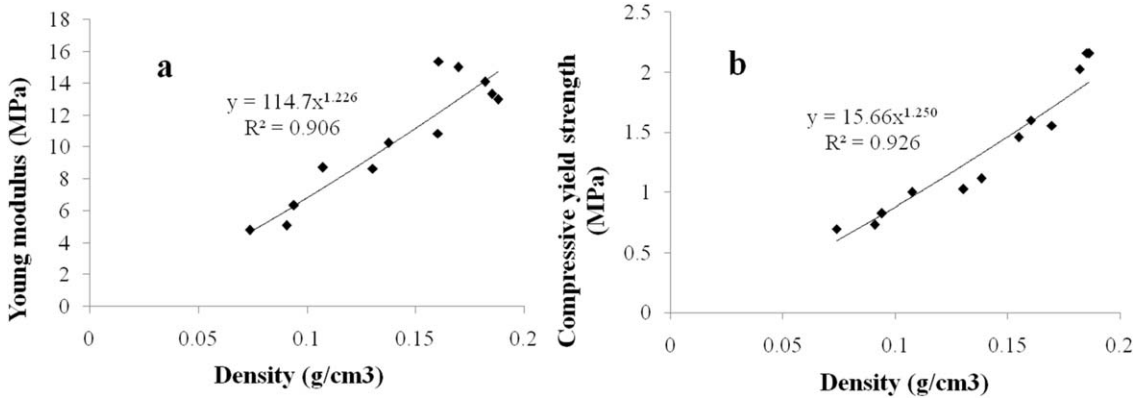

Figure 10. (a) *E* and (b) compressive yield strength versus density.

gelation and the replacement of liquid in gel with gas with lyophilization. The incorporation of nanoclay into the cellulose matrix caused a reduction in the mean pore size diameter; this strongly influenced the density, porosity, and mechanical properties. According to the XRD patterns, a complete intercalation of the cellulosic matrix into clay interlayer galleries reinforced the modulus and compressive strength of the foams. In general, the obtained properties for materials formed from cellulose allow their use as a potential alternatives to petroleum-based plastic materials for food-packaging applications. However, more research is needed to improve the properties and extend their applications.

ACKNOWLEDGMENTS

This work was supported by the Center for International Scientific Studies & Collaboration and the French Embassy in Tehran.

REFERENCES

1. Fischer, F.; Rigacci, A.; Pirard, R.; Berthon-Fabry, S.; Achard, P. *Polymer* **2006**, *47*, 7636.
2. Strey, R.; Klostermann, M.; Kramer, L.; Schwering, R.; Sottmann, T. U.S. Pat. 0,174,192 (**2011**).
3. Tomoyuki, F.; Toshimasa, Y.; Kozo, N.; Osato, M. *J. Membr. Sci.* **2001**, *187*, 171.
4. Sehaqui, H.; Zhou, Q.; Berglund, L. A. *Compos. Sci. Technol.* **2011**, *71*, 1593.
5. Gavillon, R.; Budtova, T. *Biomacromolecules* **2008**, *9*, 269.
6. Yang, Q.; Qin, X.; Zhang, L. *Cellulose* **2011**, *18*, 681.
7. Jin, Z.; Wang, S.; Wang, J.; Zhao, M. *J. Appl. Polym. Sci.* **2012**, *125*, 704.
8. Mao, Y.; Zhou, J.; Cai, J.; Zhang, L. *J. Membr. Sci.* **2006**, *279*, 246.
9. Sescousse, R.; Gavillon, R.; Budtova, T. *Carbohydr. Polym.* **2011**, *83*, 1766.
10. Consuelo, V.; Schmidt, R.; Laurindo, J. B. *Braz. Arch. Boil. Technol.* **2010**, *53*, 185.
11. Bendahou, D.; Bendahou, A.; Seantier, B.; Grohens, Y.; Kaddami, H. *Ind. Crops Prod.* doi: 10.1016/j.indcrop.2014.11.012
12. Shi, J.; Lu, L.; Guo, W.; Zhang, J.; Cao, Y. *Carbohydr. Polym.* **2013**, *98*, 282.
13. Duchemin, B. J. C.; Staiger, M. P.; Tucker, N.; Newman, R. H. *J. Appl. Polym. Sci.* **2010**, *115*, 216.
14. Gawryla, M. D.; Van den Berg, O.; Weder, C.; Schiraldi, D. A. *J. Mater. Chem.* **2009**, *19*, 2118.
15. Jia, N.; Li, S. M.; Ma, M. G.; Sun, R. C.; Zhu, J. F. *Carbohydr. Polym.* **2012**, *88*, 179.
16. Yang, Q.; Wu, C. N.; Saito, T.; Isogai, A. *Carbohydr. Polym.* **2014**, *100*, 179.
17. Ma, H.; Zhou, B.; Li, H. S.; Li, Y. Q.; Ou, S. Y. *Carbohydr. Polym.* **2011**, *84*, 383.
18. Yan, Z.; Chen, S.; Wang, H.; Wang, B.; Wang, C.; Jiang, J. *Carbohydr. Res.* **2008**, *343*, 73.
19. Ma, P. X.; Choi, J. W. *Tissue Eng.* **2001**, *7*, 23.
20. Mikos, A. G.; Thorsen, A. J.; Czerwonka, L. A.; Bao, Y.; Langer, R.; Winslow, D. N.; Vacanti, J. P. *Polymer* **1994**, *35*, 1068.
21. Ahmadzadeh, S.; Nasirpour, A.; Keramat, J.; Hamdami, N.; Behzad, T.; Desobry, S. *Colloids Surf. A* **2015**, *468*, 201.
22. Tunç, S.; Duman, O. *Appl. Clay Sci.* **2010**, *48*, 414.
23. Li, R.; Zhang, L.; Xu, M. *Carbohydr. Polym.* **2012**, *87*, 95.
24. Gindl, W.; Keckes, J. *Polymer* **2005**, *46*, 10221.
25. Aaltonen, O.; Jauhiainen, O. *Carbohydr. Polym.* **2009**, *75*, 125.
26. Salgado, P. R.; Schmidt, V. C.; Molina,; Ortiz, S. E.; Mauri, A. N.; Laurindo, J. B. *J. Food Eng.* **2008**, *85*, 435.
27. Rabek, J. F. Experimental Methods in Polymer Chemistry; Wiley-Interscience: Chichester, United Kingdom, **1980**; p 505.
28. Shanshan, G.; Jianqing, W.; Zhengwei, J. *Carbohydr. Polym.* **2012**, *87*, 1020.
29. Azizi, H.; Morshedian, J.; Barikani, M.; Wagner, M. H. *Express Polym. Lett.* **2010**, *4*, 252.
30. Slavutsky, A. M.; Bertuzzi, M. A.; Armada, M. *Braz. J. Food Technol.* **2012**, *15*, 208.
31. Abdullah, M. A.; Mamat, M.; Awang, M.; Kusrini, E.; Mubin, F. N. A.; Sudin, N. H. *Int. J. Technol.* **2013**, *2*, 129.
32. Kim, S. W.; Cha, S. H. *J. Appl. Polym. Sci.* **2014**, *131*, 1.
33. Chivrac, F.; Pollet, E.; Avérous, L. *Mater. Sci. Eng.* **2010**, *67*, 1.
34. Chung, Y. L.; Ansari, S.; Estevez, L.; Hayrapetyan, S.; Giannelis, E. P.; Lai, H. M. *Carbohydr. Polym.* **2010**, *79*, 391.
35. Wilhelm, H. M.; Sierakowski, M. R.; Souza, G. P.; Wypych, F. *Carbohydr. Chem.* **2003**, *52*, 101.
36. Majdzadeh-Ardakani, K.; Navarchian, A.; Sadeghi, F. *Carbohydr. Polym.* **2010**, *79*, 547.
37. Isogai, A.; Usuda, M.; Kato, T.; Uryu, T.; Atalla, R. *Macromolecules* **1989**, *22*, 3168.
38. Lawton, J. W.; Shogren, R. L.; Tiefenbacher, K. F. *Ind. Crops Prod.* **2004**, *19*, 41.
39. Glenn, G. M.; Orts, W. J.; Nobes, G. A. R. *Ind. Crops Prod.* **2001**, *14*, 201.
40. Soykeabkaew, N.; Supaphol, P.; Rujiravanit, R. *Carbohydr. Polym.* **2004**, *58*, 53.